ALTIN GJEVORI

Phase Formation of Photoactive TiO2 Thin Films by Metal Plasma Immersion Ion Implantation and Deposition

Engelsdorfer Verlag
Leipzig
2014

This work was prepared from February 2007 until March 2010 at the Leibniz-Institut für Oberflächenmodifizierung e. V. Leipzig, Germany.

Supervisors:
Prof. Dr. Dr. h.c. Bernd Rauschenbach
PD. Dr. Stephan Mändl
Prof. Dr. Halil Sykja

Bibliografische Information durch die Deutsche Nationalbibliothek:
Die Deutsche Nationalbibliothek verzeichnet diese Publikation in der Deutschen Nationalbibliografie; detaillierte bibliografische Daten sind im Internet über http://dnb.dnb.de abrufbar.

ISBN 978-3-95488-746-0

Hergestellt in Leipzig, Germany (EU)
www.engelsdorfer-verlag.de

10,00 Euro (D)

TABLE OF CONTENTS

CHAPTER 1 Introduction

Titanium dioxide (TiO_2) belongs to the family of transition metal oxides. Among the semiconductors, TiO_2 (E_g = 3.2eV) has proven to be the most suitable for widespread environmental applications, since it is biologically and chemically inert; it is stable with respect to photocorrosion and chemical corrosion; and it is inexpensive. Photoinduced processes are studied in a manifold ways and various applications have been developed since their first description. Beside an electrical use of this energy in solar cells, chemical effects (photochemical catalysis) or surface changes of the catalyst itself (superhydrophilicity) are observed. Titanium dioxide is one of the most important and most widely used compounds in all these application areas. By far, the most active field of TiO_2 photocatalysis is the photodegeneration of organic compounds. TiO_2 has become a photocatalyst in environmental decontamination for a large variety of organics, viruses, bacteria, fungi, algae, and cancer cells, which can be totally degraded and mineralized to CO_2, H_2O, and harmless inorganic anions. The ability to control photocatalytic activity is important in many other applications including utilization of TiO_2 in paint pigments and cosmetics.

However, to obtain the active phases anatase or rutile, conventional thin film deposition techniques need substrate temperatures of at least 400 – 700 °C, precluding the use of many temperature sensitive substrates, especially polymers. Using ion assisted deposition, it is known that the athermal energy provided by the impinging ions within the immediate surface region will results in a very short and spatially confined thermal spike, thus allowing the grows of high temperature phases while the substrate remains at room temperature.

TiO_2 can be prepared in the form of powder, crystals, or thin films. While powders are frequently utilized, thin films prepared by different methods, as magnetron sputter deposition, plasma immersion ion implantation and metal arc deposition, are also under investigation.

Metal Plasma Immersion Ion Implantation and Deposition (MEPIIID) is a relatively new method for surface modification of materials. Using this method, a pulsed regime is employed with accelerated, energetic ions arriving on the substrate during the high voltage pulses and low energy, respective hypersonic ions from the cathodic arc used to generate the Ti ions, between the pulses. Compared to continuous bombardment with 500-1500 eV ions, in this

pulsed mode the total sputter rate of the growing film by the impinging ions is reduced. Oxygen gas backfill leads to a partial transfer of the kinetic energy from Ti ions to oxygen molecules during the transit from the cathode towards the substrate, thus partially ionizing the oxygen molecules. Furthermore, neutral oxygen atoms are preferentially adsorbed on the reactive TiO_2 surface and included in the film growth.

The aim of this work has been the formation of photoactive titanium dioxide thin films on temperature sensitive substrates using energetic ion bombardment to supply the necessary energy for anatase or rutile phase formation as well as heating the substrate up to 300 °C. According to published literature data on the phase formation of TiO_2, an average energy of 20 eV per deposited particle corresponds to substrate temperature around 700 °C. Using MEPIIID to accelerate the ions, a large variety of parameters is available to tailor the ion bombardment.

After reviewing the properties, structure and photoactive properties of TiO_2 in chapter 2, the basics of PIII and MePIIID are described in chapter 3. Experimetal setup used in this work and short overview of the used analytic techniques are presented in chapters 4 and 5. The main part of this thesis is presented in chapter 6 and 7.

In chapter 6 the results obtained from investigations of structure, morphology and photoactivity of the samples produced by MePIIID at room temperature, are presented and discussed. At a typical pulse length of 10 – 30 µs and duty cycles of 5 – 15%, average particle energies of up to 250 eV were achieved for 3 – 5 kV pulse voltage when taking the average charge state and ionized fraction into account. Phase formation, texture and morphology are investigated using SEM, TEM, X-ray diffraction and Raman spectroscopy. Silicon, Silicon oxide and fused silica wafers are used as substrates for these investigations. The photo-induced activity was evaluated into ways: (i) measuring the surface energy of the thin films using two different liquids (to allow the derivation of the surface energy and the polar/disperse fractions from the contact angle) as a function of UV illumination (time and intensity); (ii) determination of the decomposition rate of methylene blue, an organic model substance, used for evaluating the photo-activity of TiO_2. Thus, the deposited energy is supposed to be sufficient to induce the formation of the high temperature rutile phase. However, the nucleation processes were normally occurring on a much shorter timescale. Thus, it was established that rutile nucleates during the pulses and anatase or an amorphous phase between the pulses with a subsequent growth of both phases. Additionally, a variation

of the pulse voltage and the duty cycle was performed to keep the average energy constant while the pulse voltage was varied. Beside the athermal energy deposition by the energetic ions, damage formation proportional to the ion energy was occurring, which is especially critical for low temperatures and high ion energies as the subsurface damage cannot be annealed under these conditions, in contrast to the surface damage.

In chapter 7 the results obtained from investigations on TiO_2 thin film deposited with additional substrate heating using a different experimental setup from above chapter are presented. The energy/temperature phase diagram available in the literature which quantifies the replacement of thermal substrate heating with energetic ions was provided to exemplify the basic mechanisms during thin film deposition, especially the phase formation. However, as secondary effects as grain boundaries or crystallite size with their corresponding electronic defects are playing an important role in the photo-induced activity, a detailed investigation on temperature effects, especially annealing of defects and enhancement of crystallite growth with a reduced density of grain boundaries was performed.
These latter effects cannot be produced by ion bombardment alone, thus a process optimization with the substrate temperature or the temperature variation during the process (e.g. high energy bombardment during the nucleation phase at low substrate temperature with a reduced energy and increased substrate heating during the following growth phase) to find the highest photo-activity of the deposited thin films. Depending on the previous results, only selected methods, which are most representative and informative on the parameters determining the photo-activity, for thin film analysis are used during this stage.
Finally in chapter 8, a summary and conclusions are presented.

CHAPTER 2 Titanium Dioxide

In this chapter, after a short presentation of TiO_2 properties and applications, a description of TiO_2 structure with focus to photoactive properties is introduced.

2.1 TiO_2 Properties

TiO_2 has received a great deal of attention due to its chemical stability, non-toxicity, low cost, and other advantageous properties. Because of its high refractive index, it is used as anti-reflection coating in silicon solar cells and in many thin-film optical devices [1]. Due to its hemocompatibility with the human body, TiO_2 is used as a biomaterial (as bone substituent and reinforcing mechanical support) [2, 3, 4, 5, 6, 7, 8]. TiO_2 is also used in catalytic reactions [9] acting as a promoter, a carrier for metals and metal oxides, an additive, or as a catalyst.

Rutile is investigated as a dielectric gate material for MOSFET devices as a result of its high dielectric constant ($\varepsilon > 100$) [10, 11], and doped anatase films (using Co) might be used as a ferromagnetic material in spintronics [12, 13]. In batteries, the anatase form is used as an anode material in which lithium ions can intercalate reversibly [14]. For solar cell applications, the anatase structure is preferred over the rutile structure, as anatase exhibits a higher electron mobility, lower dielectric constant, lower density, and lower deposition temperature.

The primary criterion for good semiconductor photocatalysts for organic compound degradation is that the redox potential of the $H_2O/{\cdot}OH$ ($OH^- = {\cdot}OH + e^-$; $E^o = -2.8$ V) couple lies within the bandgap domain of the material and that the material is stable over prolonged periods of time. Among various possible semiconductors such as metal oxides (TiO_2, ZnO, CeO_2, etc) and metal sulfide (CdS, ZnS, etc), titanium dioxide TiO_2 ($E_g = 3.2$ eV) has proven to be the most suitable for the photodegradation of toxic organic molecules due to its excellent photocatalytic performance with maximum quantum yields [15]. Semiconductor photocatalysis with a primary focus on TiO_2 as a durable photocatalyst has been applied to a variety of problems of environmental interest in addition to water and air purification, for the destruction of microganisms [16, 17], for the inactivation of cancer ce11s [18, 19], for the photosplitting of water to produce hydrogen gas [20, 21, 22, 23, 24] and for the cleanup of oil spills [25, 26, 27].

2.2 TiO_2 Phase Diagram

Titanium builds some stable oxides. In figure 2.1 is given the phase diagram of the titanium-oxygen [28].

The most important data from the above phase diagram are:

- Oxygen dissolves up to 30 atom % in the α-titanium phase
- TiO crystallizes in NaCl missing state structure and can be found in a non-stoichiometric form of larger phase width TiO_x ($0.70 \leq x \leq 1.30$).
- Ti_2O_3 has a corundum structure and above 200°C shows a transition from semiconductor to conductor.
- With increasing oxygen concentration oxide phases of Magnelli-type (Ti_nO_{2n-1}, with $4 \leq n \leq 9$) are formed. Here plates with a structure similar to Rutile under crystallographic shearing strain are connected to each other, thus stint oxygen atoms by sharing of more edges between neighbor octahedra. These phases are semiconductors beside the Ti_4O_7 which is similar to metals.
- The most stable phase TiO_2 at normal pressure is rutile.

The last one requires an explanation because in the nature one finds three stable TiO_2 phases: rutile, anatase and brookite. The transition from brookite/anatase in rutile at higher

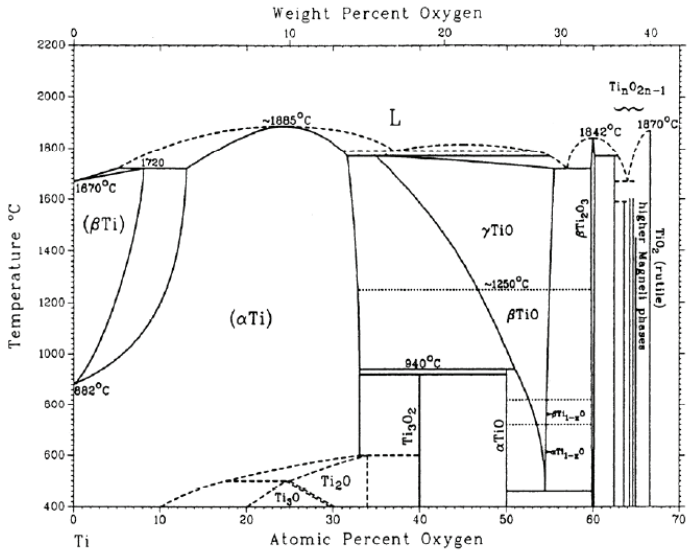

Figure 2.1: *TiO_2 phase diagram*

temperatures is not reversible [28]. Therefore rutile is thermodynamically the most stable form of TiO_2 at normal pressure and 5 – 12 kJ/mol more stable than anatase [29].

2.3 The Structure of TiO_2

As stated, titanium dioxide crystallizes in three major different structures; rutile (tetragonal, $D_{4h}^{14} - P4_2/mnm$, a = b = 0.459 nm, c = 0.296 nm [30]), anatase (tetragonal, $D_{4h}^{19} - I4_1/amd$, a = b = 0.379 nm , c = 0.954 [31]) and brookite (rhombohedrical, $D_{2h}^{15} - Pbca$, a = 0.545 nm, b = 0.917 nm, c = 0.514 nm) [32]. However, only rutile and anatase play any role in the applications of TiO_2 and are of any interest here. The unit cells of rutile and anatase are shown in figure 2.2, and the stacking octahedra of titanium dioxide major structures are depicted in figure 2.3.

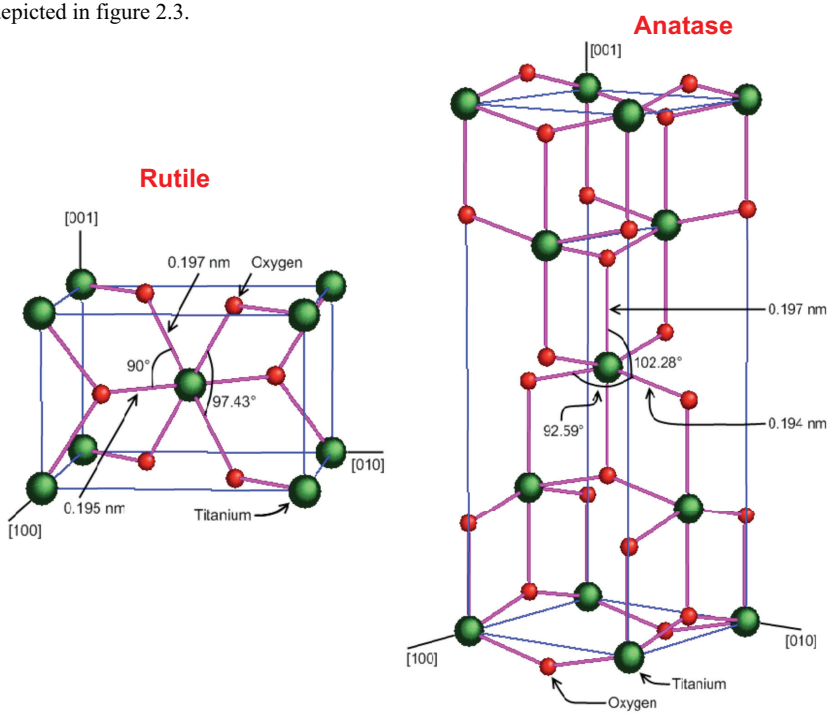

Figure 2.2: *Bulk structures of rutile and anatase. The tetragonal bulk unit cell of rutile has the dimensions, a = b = 0.459 nm, c = 0.296 nm, and the one of anatase a = b = 0.379 nm, c = 0.954 nm. In both structures, slightly distorted octahedra are the basic building units. The bond lengths and angles of the octahedrally coordinated Ti atoms are indicated.*

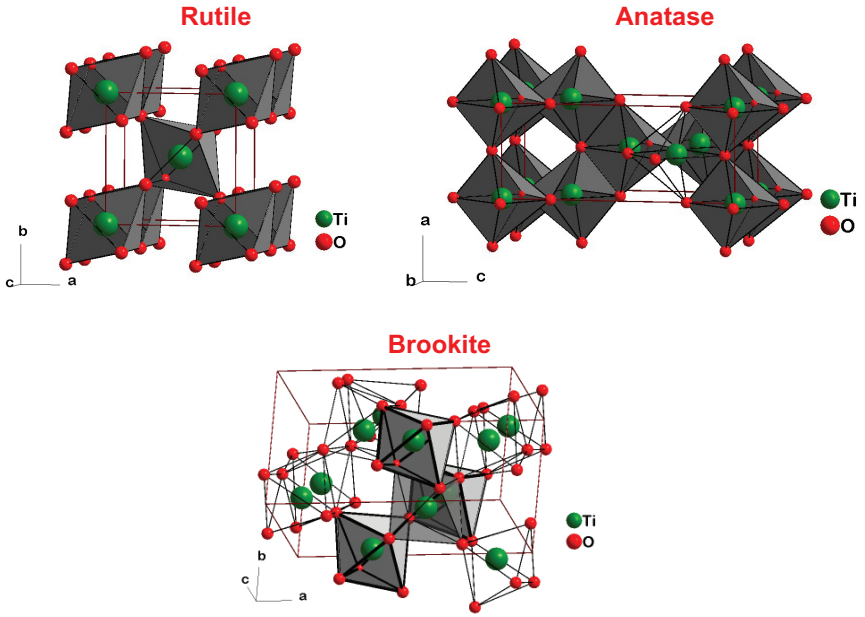

Figure 2.3: *The stacking of the octahedra in rutile, anatase and brookite structures*.

The structures of rutile, anatase and brookite can be discussed in terms of (TiO_2^{6-}) octahedrals. The three crystal structures differ by the distortion of each octahedral and by the assembly patterns of the octahedral chains. In rutile, neighboring octahedra share one corner along ‹110› – type directions, and are stacked with their long axis alternating by 90°. In anatase the corner-sharing octahedra form (001) planes. They are connected with their edges with the plane of octahedra below. In brookite, both vertices and edges are connected.

Particle size experiments affirm that the relative phase stability may reverse when particle sizes decrease to sufficiently low values due to surface-energy effects (surface free energy and surface stress, which depend on particle size) [33]. If the particle sizes of the three crystalline phases are equal, anatase is most thermodynamically stable at sizes less than 11 nm, brookite is most stable between 11 and 35 nm, and rutile is most stable at sizes greater than 35 nm [34].

The enthalpy of the anatase → rutile phase transformation is low. A survey of the literature reveals widespread disagreement, with values ranging from -1.3 to -6:0 ± 0.8 kJ/mol [35, 36, 37]. Kinetically, anatase is stable, i.e., its transformation into rutile at room temperature is so

slow that the transformation practically does not occur. At macroscopic scale, the transformation reaches a measurable speed for bulk TiO_2 at T > 600 °C [38, 39, 40]. The monotropic [41] anatase → rutile conversion has been studied for both mechanistic and application-driven reasons, because the TiO_2 phase (i.e., anatase or rutile) is one of the most critical parameters determining the use as a photocatalyst [42].

2.4 Photoactivity of TiO_2

The photoactivity of TiO_2 is one of its technological most attractive properties. The creation of electron-hole pairs through irradiation of light, either in TiO_2 itself, or in adsorbed molecules, and the following chemical or electron transfer reactions are at the heart of TiO_2 based photodevices applied in a range of areas. All photoinduced phenomena are activated by an input of super-band gap energy to the semiconductor TiO_2. Absorption of a photon with enough energy leads to a charge separation due to an electron promotion to the conduction band and a generation of a hole (h^+) in the valence band. The subsequent mode of action of the photogenerated electron–hole pair (e^-–h^+), determines which of the phenomena is the dominant process, because even if they are intrinsically different processes, they can and in fact take place concomitantly on the same TiO_2 surface. Photocatalysis is a well-known process and is mostly employed to degrade or transform (into less harmful substances) organic and inorganic compounds and even microorganisms. The recently discovered wettability, termed as 'superhydrophilicity' [43], presents a large range of applications in cleaning and anti-fogging surfaces. The detailed material properties required for enhanced efficiency are different from each other. For enhanced photocatalysis, deep electron traps and high surface acidity are needed to lengthen the lifetime of photoexcited electrons and holes and to ensure better adsorption of organic substances on the surface. Meanwhile, low surface acidity and, most of all, a large quantity of Ti^{3+} is essential for hydrophilic surface conversion. These differences are related to the fact that photocatalysis is more likely to be sensitive to bulk properties, while hydrophilicity can be definite as an interfacial phenomenon.

2.4.1 Photocatalysis of TiO_2

Semiconductor electronic structures are characterized by a filled valence band (VB) and an empty conduction band (CB), and can act as sensitizers for light-reduced redox processes. When a photon with an energy of *hv* matches or exceeds the bandgap energy E_g of the semiconductor, an electron e^-_{cb}, is promoted from the valence band, into the conduction band, leaving a hole, h^+_{vb}, behind. Excited state conduction-band electrons and valence-band holes

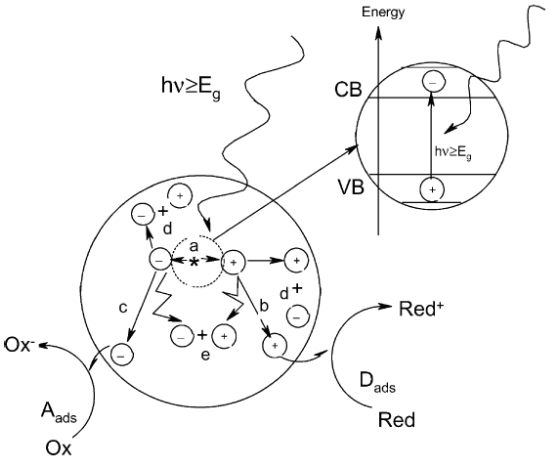

Figure 2.4: *Main processes occurring on a semiconductor particle: (a) electron–hole generation; (b) oxidation of donor (D); (c) reduction of acceptor (A); (d) and (e) electron–hole recombination at surface and in bulk, respectively [44].*

can react with electron donors and electron acceptors adsorbed on the semiconductor surface or within the surrounding electrical double layer of the charged particles or recombine and dissipate the input energy as heat, get trapped in metastable surface states. The above process in the photocatalysis is illustrated in figure 2.4.

For a semiconductor photocatalyst to be efficient, the different interfacial electron processes involving e_{cb}^- and h_{vb}^+ must compete effectively with the major deactivation processes involving $e_{cb}^- - h_{vb}^+$ recombination, which may occur in the bulk or at the surface. Ideally, a semiconductor photocatalyst should be chemically and biologically inert, photocatalytically stable, easy to produce and to use, efficiently activated by sunlight, able to efficiently catalyze reactions, cheap, and without risks for the environment or humans. Titanium dioxide (with sizes ranging from clusters to colloids to powders and large single crystals) is close to being an ideal photocatalyst, displaying almost all the above properties. The single exception is that it does not absorb visible light.

TiO_2 photocatalysis mechanism can be described as below [15]:

Charge – carrier generation

$$TiO_2 + h\nu \rightarrow e_{CB}^- + h_{VB}^+ \qquad (2.1)$$

Charge – carrier trapping

$$h_{VB}^{+} + \left[-Ti^{4+}OH\right] \rightarrow \left[-Ti^{4+}OH^{\bullet+}\right]$$
$$e_{CB}^{-} + \left[-Ti^{4+}OH\right] \leftrightarrow \left[-Ti^{3+}OH\right] \quad (2.2)$$
$$or$$
$$e_{CB}^{-} + Ti^{4+} \rightarrow Ti^{3+}$$

Charge – carrier recombination on the surface

$$e_{CB}^{-} + \left[-Ti^{4+}OH^{\bullet+}\right] \rightarrow Ti^{4+}OH$$
$$h_{VB}^{+} + \left[-Ti^{3+}OH\right] \rightarrow Ti^{4+}OH \quad (2.3)$$

Interfacial charge transfer

$$\left[-Ti^{4+}OH^{\bullet+}\right] + R_{ed} \rightarrow \left[-Ti^{4+}OH\right] + R_{ed}^{\bullet+}$$
$$\left[-Ti^{3+}OH\right] + O_x \rightarrow \left[-Ti^{4+}OH\right] + O_x^{\bullet-} \quad (2.4)$$
$$Ti^{3+} + O_x \rightarrow Ti^{4+} + O_x^{\bullet-}$$

where $[-Ti^{4+}OH]$ represents a OH group of TiO2, e_{CB}^{-} is a conduction band electron, h_{VB}^{+} is a valence-band hole, Red is an electron donor (i.e., reductant), Ox is an electron acceptor (i.e., oxidant), $[-Ti^{4+}OH^{\bullet+}]$is the surface-trapped VB hole (i.e., surface-bound hydroxyl radical), and $\left[-Ti^{3+}OH\right]$ is the surface-trapped CB electron.

Above reactions may be summarized as follows:

$$(Ox_1)_{ads} + (Red_2)_{ads} \xrightarrow{h\nu > E_g} Red_1 + Ox_2 \quad (2.5)$$

Depending on whether the sign of the change in Gibbs free energy (ΔG°) of the above reaction is negative or positive, the semiconductor-sensitized reaction may be an example of photocatalysis or photosynthesis, respectively [45].

Both crystal structures, anatase and rutile, are commonly used as photocatalyst, with anatase showing a greater photocatalytic activity [42, 46] for most reactions. It has been suggested that this increased photoreactivity is due to anatase's slightly higher Fermi level, lower capacity to absorb oxygen and higher degree of hydroxylation (i.e., number of hydroxy groups on the surface) [46]. Reactions in which both crystalline phases have the same photoreactivity [47] or rutile a higher one [48] are also reported. Furthermore, there are also studies which claim that a mixture of anatase (70–75%) and rutile (30–25%) is more active than pure anatase [49, 50]. The disagreement of the results may lie in the intervening effect of various coexisting factors, such as specific surface area, pore size distribution, crystal size, and preparation methods, or in the way the activity is expressed.

2.4.2 Photoinduced Superhydrophilicity

UV illumination of TiO_2 may induce a patchwork of superhydrophilicity (i.e., photoinduced superhydrophilicity or PSH) across the surface that allows both water and oil to spread [51, 43]. This PSH is accompanied by photocatalytic activity, as both phenomena have a common ground; so the surface contaminants will be either photomineralized or washed away by water. One possible application is self-cleaning windows. PSH involves reduction of Ti(IV) cations to Ti(III) by electrons and simultaneous trapping of holes at lattice sites (usually bridging oxygen) or close to the surface of the semiconductor. Such trapped holes weaken the bond between the associated titanium and lattice oxygen, allowing oxygen atoms to be liberated, thus creating oxygen vacancies. The subsequent dissociative adsorption of water at the site renders it more hydroxylated. An increased amount of chemisorbed –OH leads to an increase of van der Waals forces and hydrogen bonding interactions between H_2O and –OH. Water can easily spread across the surface and hydrophilic properties will be enhanced [52, 53] (figure 2.5). Water adsorption does not occur uniformly but produces an amphiphilic surface with alternating hydrophilic and oleophilic regions at the scale of several nanometers (usually <10 nm in size) [51]. The hydrophilic domains align along the bridging oxygen sites. The reduced sites can be reoxidized by air and the weakly bound hydroxyl groups reactively desorbs (over some time, typically days in the dark) from the surface that returns to a more hydrophobic form. The longer the surface is illuminated with UV light, the smaller the contact angle for water becomes (a contact angles close to zero mean that water spreads perfectly across the surface). As far as the geometry of the surface is concerned, the hydrophilic properties are known to be enhanced by fine surface roughness [52, 53, 54, 55].

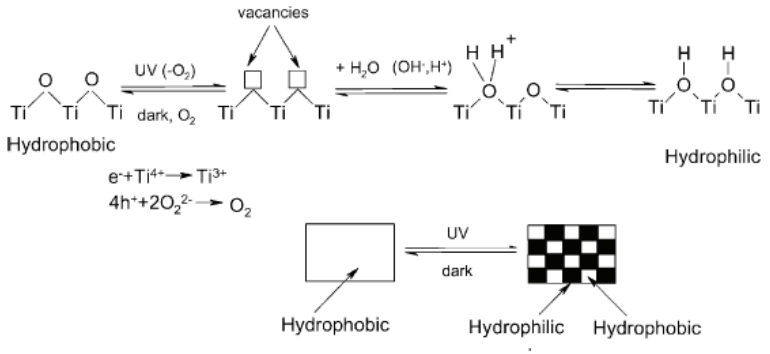

Figure 2.5: *Mechanism of photoinduced superhydrophilicity of TiO_2.[56]*

PSH was found to be of primary commercial importance due to the anti-fogging and self-cleaning properties of the deposits.

CHAPTER 3 Plasma Immersion Ion Implantation and Metal Plasma Immersion Ion Implantation and Deposition

Many methods are used for the preparation of TiO_2 in the form of powder, crystals or thin films, as extensively reviewed in the literature [56]. Methods correlated with the modification of surfaces are an attractive way to achieve the desired property at the surface of any bulk material. Surface modifications can be done by alloying/mixing elements at the surface of bulk materials or by an adherent overlayer on bulk materials. Plasma immersion ion implantation is one among the surface modification methods, which was developed about 20 years ago [57]. PIII is an emerging technology for the surface modification of semiconductors, metals and insulators. Materials to be treated are immersed in plasma and negative high voltage pulses are applied to the substrate holder. The positive ions are extracted from the plasma and accelerated towards the whole surface simultaneously. This technology offers a sufficiently uniform ion bombardment of components, there is no need for ion beam rastering as in conventional ion implanters, as well as providing a more simple way to treat large surface areas in a short time and cost-effective way. In the first section of this chapter the basic processes when energetic ions enter a solid, like energy loss per unit length and range, radiation damage and thermal spike, are presented. Furthermore, the principles of cathodic arc evaporation and MePIIID as a variation of PIII (where metal ions generated from cathodic arc evaporation are used), used in this work, are described.

3.1 Interaction of Ions and Electrons with Solid Surfaces

When an energetic atom or ion interacts with other particles, scattering processes occur. Elastic interactions with other atoms and inelastic scattering with electrons can be distinguished. For ion implantation within the laboratory reference system, kinetic energy is dissipated in both channels via nuclear collisions and electronic excitation, respectively. The energy loss or stopping power per length unit in the target can be given as the sum of nuclear (n) and electronic (e) stopping powers [58, 59]:

$$\frac{dE}{dx} = \left(\frac{dE}{dx}\right)_n + \left(\frac{dE}{dx}\right)_e = -N\left[S_n(E) + S_e(E)\right] \tag{3.1}$$

where N is the number density of atoms in the medium, $S_n(E)$ and $S_e(E)$ are the so-called nuclear and electronic cross sections. $S_n(E)$ determines the energy loss due to elastic collisions of the penetrating ion with target atoms and $S_e(E)$ determines the energy loss due to inelastic

processes (excitations of bound electrons of target atoms or bond breaking in a target consisting of molecules). This separation into elastic and inelastic processes can be made due to the large mass difference between ions and electrons.

An approximation for the nuclear stopping cross-section can be derived from an appropriate screened Coulomb potential [60, 61]:

$$V(r) = \frac{Z_1 Z_2 e^2}{r} \Phi\left(\frac{r}{a}\right) \tag{3.2}$$

Where Φ is the so-called screening function, which screens the repulsive Coulomb forces of the nuclei, due to the partial shielding by the surrounding electron cloud. For shorter interaction distances, less screening is observed. For the commonly used krypton-carbon (Kr-C) potential [62], Φ has the form:

$$\Phi(x) = 0.190945e^{-0.131825x} + 0.473674e^{-0.63717x} + 0.335381e^{-1.919249x} \tag{3.3}$$

$$x = \frac{r}{a_L} \qquad a_L = 0.8854a_O\left(Z_1^{2/3} + Z_2^{2/3}\right)^{-1/2} \qquad a_O = 0.0529nm \tag{3.4}$$

Where a_L ist the Lindhard screening radius for the Tomas-Fermi interaction between atoms and a_O is the Bohr radius.

Following the notation of Lindhard et al [58, 59, 60], the nuclear stopping power then can be expressed:

$$\left(\frac{dE}{dx}\right)_n = 509.6\frac{\rho Z_1 Z_2 M_1 s_n(\varepsilon)}{M_2(M_1 + M_2)\left(Z_1^{2/3} + Z_1^{2/3}\right)^{1/2}} (eV \quad nm^{-1}) \tag{3.5}$$

where M_1 is the projectile mass, M_2 is the target atom mass, ρ is the density (g cm-3) and $s_n(\varepsilon)$ is the reduced stopping cross section. An analytical expression for $s_n(\varepsilon)$ based on Kr-C potential [62,63, 64, 65] was suggested by Wilson et al [64]. Another analytical expression of $s_n(\varepsilon)$ corresponds to the so-called Ziegler-Biersack-Littmark (ZBL) or universal potential [63]. Electronic stopping does only cause small scattering angles of the penetrating particle, because of the relative small electron mass, nevertheless a noticeable energy loss is recorded. At low projectile energies, following the so-called Lindhard-Scharff (LS) regime [59, 60, 63], the electronic stopping power becomes:

$$\left(\frac{dE}{dx}\right)_e = 231.6\rho Z_1^{1/6}\frac{Z_1 Z_2}{\left(Z_1^{2/3} + Z_1^{2/3}\right)^{3/2} M_2\sqrt{M_1}}\sqrt{E(keV)}(eV \quad nm^{-1}) \tag{3.6}$$

Also the electronic stopping cross-section is often expressed in a dimensionless reduced form $s_e(\varepsilon)$.

The total path length or range of the ion can be calculated by integration over the energy losses:

$$R(E) = \int dx = -\int_0^E \frac{dE}{\left[dE/dx\right]_n + \left[dE/dx\right]_e} \tag{3.7}$$

Using the above equations in combination with the Kr-C potential, different energy losses and ranges can get estimates.

Recoil atoms (called primary knock-on atoms or PKAs) from collisions between the penetrating particle and atoms of the solid will, if sufficiently energetic, create secondary and higher-generation recoils and thus a collision cascade is produced (figure 3.1).

This leads to a distribution of vacancies, interstitial atoms and other type of lattice disorder in the region around the incident ion track. As the number of the incident ions increases, the individual disordered regions begin to overlap, and a heavily damaged layer or an amorphous region if formed. According to the radiation damage theories, a lattice atom struck by an energetic ion or recoiling target atom must receive a minimum amount of energy in the collision to be displaced from its lattice site. The minimum energy required to displace the lattice atom represents the displacement threshold and is called the displacement energy E_d. If a lattice atom in a collision receives an energy greater than E_d a vacancy and an interstitial (Frenkel pair or Frenkel defect) are formed (figure 3.1). The average number of displaced atoms in a cascade produced by a primary knock-on of energy E is the displacement damage function $N_d(E)$. A simple estimate was given by Kinchin and Pease [66], which gives for energies up to energies, where electronic stopping can be neglected (M_2keV, i.e. 64 keV for Cu):

$$N_d(E) = \begin{array}{ccc} 0 & & E < E_d \\ 1 & for & E_d < E < 2E_d \\ E/2E_d & & 2E_d < E \end{array} \tag{3.8}$$

Equation (3.8) gives the number of displaced atoms produced by a PKA.

Another measure of irradiation damage is displacements per atom or dpa. A unit of 1 dpa means that, on average, every atom in the irradiated volume has been displaced once from its equilibrium lattice site.

Starting at energies of a few 10 eV the impinging ions have enough energy to create primary recoil atoms, which can be emitted from the target when they are located close to the surface and their momentum vectors points back to the surface. This leads to an erosion of the surface and is termed sputtering [67, 68]. Sputtering is the dominant process under ion impact, resulting in an effective surface erosion, in the energy range from 1 keV up to a few 10 keV.

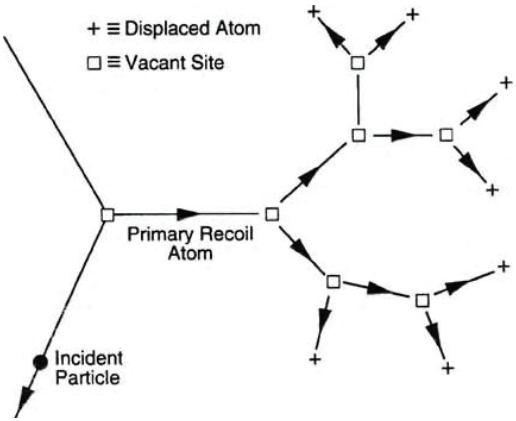

Figure 3.1: *Schematic of the formation of a collision cascade and defect creation by a primary recoil atom (PKA) [69].*

During sputtering or surface erosion neutral, excited as well as ionized atoms, molecules and clusters are ejected, the bombarding particles are in part reflected, electrons as well as radiation can be emitted from the surface or from excited sputtered particles in front of the surface. The composition of the sputtered particle flux can change drastically depending whether oxygen or other electro-negative atoms are adsorbed or incorporated in the surface from almost exclusively neutral atoms and clusters to a large contribution of ions and excited atoms.

For high energy implantations where a large amount of energy is dissipated in a small volume, a thermodynamic approximation may be used to describe collective processes. A spike is defined as a high density cascade that possesses a limited volume in which the majority of atoms are temporarily in motion [70]. This highly damaged volume of material, composed of a core of vacancies surrounded by a shell of interstitial atoms (figure 3.2), is referred to as a displacement spike. In the spike regime the density of moving atoms is so high, that essentially all atoms in the “spike volume” are moving and thus collisions are dominantly between moving atoms.

At the point when the displacement spike comes to an end, the energy will be dissipated as lattice vibrations or heat. This period of lattice heating is known as the thermal spike phase of the collision cascade and may exists for several picoseconds before being quenched to ambient temperature. For a Maxwell-Boltzmann distribution of energy, the temperature is related to the mean deposited energy density in the spike by: